JACS
JOURNAL OF THE AMERICAN CHEMICAL SOCIETY

Communication

pubs.acs.org/JACS

Proton Coupled Electronic Rearrangement within the H-Cluster as an Essential Step in the Catalytic Cycle of [FeFe] Hydrogenases

Constanze Sommer, Agnieszka Adamska-Venkatesh, Krzysztof Pawlak, James A. Birrell, Olaf Rüdiger, Edward J. Reijerse,* and Wolfgang Lubitz*

Max-Planck-Institut für Chemische Energiekonversion, Stiftstrasse 34-36, 45470 Mülheim/Ruhr, Germany

Supporting Information

ABSTRACT: The active site of [FeFe] hydrogenases, the H-cluster, consists of a [4Fe−4S] cluster connected via a bridging cysteine to a [2Fe] complex carrying CO and CN^- ligands as well as a bridging aza-dithiolate ligand (ADT) of which the amine moiety serves as a proton shuttle between the protein and the H-cluster. During the catalytic cycle, the two subclusters change oxidation states: $[4Fe{-}4S]_H^{2+} \Leftrightarrow [4Fe{-}4S]_H^{+}$ and $[Fe(I)Fe(II)]_H \Leftrightarrow [Fe(I)\text{-}Fe(I)]_H$ thereby enabling the storage of the two electrons needed for the catalyzed reaction $2H^+ + 2e^- \rightleftarrows H_2$. Using FTIR spectro-electrochemistry on the [FeFe] hydrogenase from *Chlamydomonas reinhardtii* (*Cr*HydA1) at different pH values, we resolve the redox and protonation events in the catalytic cycle and determine their intrinsic thermodynamic parameters. We show that the singly reduced state H_{red} of the H-cluster actually consists of two species: $H_{red} = [4Fe{-}4S]_H^{+} - [Fe(I)Fe(II)]_H$ and $H_{red}H^+ = [4Fe{-}4S]_H^{2+} - [Fe(I)Fe(I)]_H$ (H^+) related by proton coupled electronic rearrangement. The two redox events in the catalytic cycle occur on the $[4Fe{-}4S]_H$ subcluster at similar midpoint-potentials (−375 vs −418 mV); the protonation event ($H_{red}/H_{red}H^+$) has a $pK_a \approx 7.2$.

Hydrogenases catalyze the conversion of protons and electrons into molecular hydrogen (H_2) using the abundant metals Ni and/or Fe in their active site.[1] [FeFe] hydrogenases are particularly active in both hydrogen production (up to 8700/s) and oxidation (up to 150 000/s).[2,3] The active site of these enzymes, the "H-cluster", is composed of a "classical" cubane [4Fe−4S] cluster and a unique [2Fe] cluster coordinated by three CO and two CN^- ligands as well as an aza-dithiolate (ADT) ligand bridging the two iron atoms. The two subclusters are connected through a bridging cysteine side group coordinating $[4Fe{-}4S]_H$. The iron of the $[2Fe]_H$ subsite distal to $[4Fe{-}4S]_H$, Fe_d, is five-coordinate in most redox states and has an open coordination site where substrates (H_2 and protons) as well as inhibitors (e.g., CO) can bind (Figure 1). The amino headgroup of the ADT ligand is assumed to serve as a Brønsted base that shuttles protons between the open coordination site and the proton channel of the enzyme.[1] Three well characterized redox states of the H-cluster are postulated to play a role in the catalytic cycle:[4] $H_{ox} \rightleftarrows H_{red} \rightleftarrows H_{sred}$. Although H_{ox} and H_{red} are observed both in bacteria and algae,[5] H_{sred} is best characterized in algae.[4] The oxidized state H_{ox} is characterized by a mixed valence binuclear subsite: Fe(I)Fe(II) and an oxidized cubane subcluster $[4Fe{-}4S]_H^{2+}$.[6]

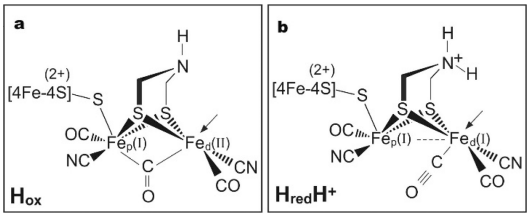

Figure 1. Structure of the H-cluster in the H_{ox} and the protonated reduced state $H_{red}H^+$.[7,8] The arrow indicates the open coordination site where hydrogen, CO and oxygen species can bind.

The reduced state H_{red} features a homovalent $[2Fe]_H$ subsite, Fe(I)Fe(I),[6] whereas a second reduction leads to the "superreduced" state H_{sred} in which the cubane subcluster is also reduced $[4Fe{-}4S]_H^{+}$.[4] In addition, the H_{ox} and H_{red} states can also bind an extrinsic CO ligand leading to the inhibited states H_{ox}−CO and H_{red}−CO.[9] Under strongly reducing conditions as well as in a mutant in which the proton transfer pathway has been blocked, the enzyme shows an FTIR signature assigned to a putative hydride state featuring an oxidized $[2Fe]_H$ core, Fe(II)Fe(II), and a terminal hydride bound to Fe_d.[10] The ordering of protonation and redox steps in the catalytic mechanism has been frequently discussed but remains largely speculative.[4,11] By studying the [FeFe] hydrogenase from *Chlamydomonas reinhardtii* (*Cr*HydA1) using pH dependent FTIR spectro-electrochemistry, we were able to resolve the redox and protonation events in the catalytic cycle. We show that the active reduced state H_{red} occurs in both protonated and unprotonated states, each with a different electronic configuration. Our spectro-electrochemical titrations allow the extraction of the intrinsic redox potentials (assuming Nernst-like behavior) as well as the pK_a for the $H_{red}/H_{red}H^+$ protonation event. These new data strongly support an "internal" PCET step connecting H_{red} and $H_{red}H^+$ and add new essential details to our understanding of the catalytic cycle.

Samples of *Cr*HydA1 were prepared[12] at pH 6.0, 7.0, 8.0, 9.0, and 10.0 showing pH dependent hydrogen production up to 600/s (700 μmol H_2/(min·mg) (see Figures S1−2). These samples were characterized using FTIR spectro-electrochemical experiments in the range −650 to −200 mV vs standard hydrogen electrode (SHE) at 288 K. Figure 2A shows FTIR

Received: December 8, 2016
Published: January 11, 2017

DOI: 10.1021/jacs.6b12636
J. Am. Chem. Soc. 2017, 139, 1440−1443

spectra at pH values and potentials highlighting the different species occurring during the electrochemical titrations.

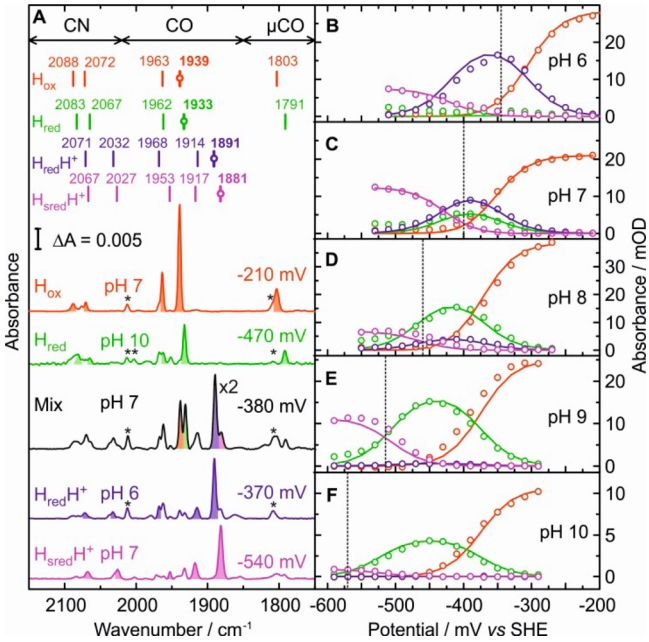

Figure 2. (A) Selected FTIR spectra recorded at optimal pH and potential, T = 288 K. (B–F). FTIR spectro-electrochemical data obtained for reductive titrations for the observed states H_{ox} (1939 cm^{-1}), H_{red} (1933 cm^{-1}), $H_{red}H^+$ (1891 cm^{-1}), $H_{sred}H^+$ (1881 cm^{-1}) at different pH. The characteristic band frequencies for each state are indicated above the spectra. The asterisks indicate the most prominent band positions of the $H_{ox/red}$–CO state that is present in small amounts in most preparations (see Figure S3–4). The dotted black lines represent the equilibrium H^+/H_2 potentials at 1 bar (100%) H_2 at each pH value (see Figure S5). The solid lines (same color code as in panel A) represent a least-squares fit to the model depicted in Figure 3. The optimized fit parameters are $pK_{ox} < 5$, $pK_{red} = 7.2 \pm 0.2$, $pK_{sred} = 9.1 \pm 0.4$, $E_1 = -375 \pm 10$ mV, $E_4 = -418 \pm 10$ mV. $E_2(H_{red}/H_{sred}) = -527 \pm 10$ mV and $E_3(H_{ox}H^+/H_{red}H^+) > -250$ mV.

It turned out that the bands at 1891 and 1933 cm^{-1}, previously assigned to the active reduced state H_{red} in *Cr*HydA1,[13] actually belong to two separate reduced states one of which (H_{red} identified by the 1933 cm^{-1} band) is dominating at pH 10 whereas the other (identified by the 1891 cm^{-1} band) reaches its maximum amplitude near pH 6. At neutral pH, both bands are visible and show identical behavior as a function of the electrochemical potential (see Figure 2C,D) which is the reason that these were originally assigned to one species.[4,9,13] We assume that the newly identified H_{red} state is protonated and refer to it as $H_{red}H^+$.

It now becomes apparent that the H_{red} state observed at pH 10 and identified by the CO stretches 1962, 1933, 1791 cm^{-1} shows great similarity with the reduced state previously observed in *Cr*HydA1-PDT,[9] i.e., a variant of *Cr*HydA1 in which the ADT ligand has been replaced with propanedithiolate (PDT) containing a methylene group instead of the amine moiety. *Cr*HydA1-PDT shows only two redox states: H_{ox}(PDT) which is almost identical in electronic structure and FTIR spectrum to the native H_{ox}(ADT) state and H_{red}(PDT) which corresponds to the native H_{red}(ADT) state identified in the current study. It can be argued that both H_{red}(PDT) and H_{red}(ADT) are characterized by a $[4Fe–4S]^+_H$ – [Fe(I)Fe(II)] configuration due to the very small red shift (3–7 cm^{-1}) of the CO bands with respect to H_{ox}(PDT/ADT), which suggests the reduction event cannot take place at the binuclear subsite.[9] In contrast, the *Cr*HydA1 $H_{red}H^+$ state observed at pH 6 is identified by the characteristic bands 1968, 1914, 1891 cm^{-1} associated with the H_{red} state previously observed for the [FeFe]-hydrogenase from *Desulfovibrio desulfuricans* (*Dd*HydAB).[14] The redox states of the H-cluster in *Dd*HydAB have been originally analyzed by Mössbauer spectroscopy[6] indicating a homovalent $[2Fe]_H$ configuration in H_{red} and an oxidized $[4Fe–4S]^{2+}_H$ subcluster. The loss of the bridging CO band in FTIR as well as the large red shift of most of the CO stretches indicates that the $[2Fe]_H$ subsite has been reduced to a homovalent [Fe(I)Fe(I)] configuration.[15,16] The transition from H_{red} to $H_{red}H^+$, therefore, involves electron transfer from the $[4Fe–4S]_H$ subcluster to the $[2Fe]_H$ subsite. Since the $H_{red}H^+$ state is only dominant at low pH, it is justified to assume that this internal electron transfer is coupled to a protonation step, presumably at the ADT ligand. This process is not a "classical" PCET reaction[17] because the electron transfer occurs within the H-cluster as an electronic rearrangement. An early DFT study by Yu et al. of the FTIR signatures of the various H-cluster states in different organisms had already pointed out that the H_{red} state reported in *Cr*HydA1 could actually consist of two species, possibly related to an electron transfer step between the two subclusters.[18] This suggestion has been validated experimentally in our current study. Furthermore, a recent low temperature Resonance Raman study on *Cr*HydA1 reported that the protonated H_{red} state can be transiently photoexcited to the unprotonated form (referred to as Hred').[19]

Proton coupled electronic rearrangement from H_{red} to $H_{red}H^+$ prepares the H-cluster for a second reduction. This reduction again takes place at the $[4Fe–4S]_H$ subcluster affording the superreduced state that we assume to be protonated at neutral pH (i.e., $H_{sred}H^+$). Taking into account two reduction steps and one protonation event we arrive at the six-state scheme of equilibria[17] (Figure 3) characterized by

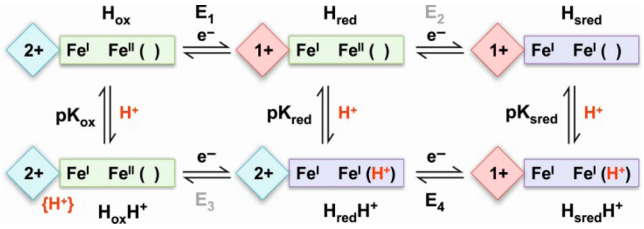

Figure 3. Equilibrium model used to analyze the pH dependent FTIR spectro-electrochemical data of *Cr*HydA1. Parameters E_2 and E_3 are taken as "overdetermined" and are calculated from the other equilibrium constants (see text and SI). The protonation of the different states is indicated by "(H^+)". For $H_{red}H^+$ and $H_{sred}H^+$, we assume that the ADT bridge is protonated.

midpoint potentials E_1...E_4 and pK_a values: pK_{ox}, pK_{red}, and pK_{sred}. Because the equilibria are interdependent not all parameters can be chosen freely. If we choose E_2 and E_3 as "overdetermined", the set of equilibria simplifies to a linear chain: $H_{ox}H^+ \rightleftarrows H_{ox} \rightleftarrows H_{red} \rightleftarrows H_{red}H^+ \rightleftarrows H_{sred}H^+ \rightleftarrows H_{sred}$ and E_2 and E_3 can be calculated from the other parameters:

$$E_3 = E_1 - \ln(10)(pK_{ox} - pK_{red})(RT)/F \quad (1)$$

DOI: 10.1021/jacs.6b12636
J. Am. Chem. Soc. 2017, 139, 1440–1443

$$E_2 = E_4 - \ln(10)(pK_{sred} - pK_{red})(RT)/F \quad (2)$$

where F is Faraday's constant, R is the gas constant, and T is the experimental temperature in Kelvin.

As explained in the SI, the calculations of the state fractions for this model, given the individual equilibrium constants, is straightforward. The equilibria between the various species are pH and potential dependent (Figure 2B–F). The FTIR spectra, however, only allow four species to be distinguished: H_{ox}, H_{red}, $H_{red}H^+$, and $H_{sred}H^+$. Protonation of the H_{ox} and H_{sred} states might induce slight changes in the electronic structure of the H-cluster leading to a blue shift (≈10 cm^{-1}) of the CO bands similar to what was reported for the putative hydride state.[10] The absence of additional $H_{ox}H^+$ and H_{sred} species in our FTIR spectra recorded in the range of pH 6.0–10.0 would suggest that pK_{ox} < 6 and pK_{sred} > 10. However, the separate observation of protonated and unprotonated species is not relevant for full modeling of the experimental data with the six-state scheme (Figure 3).[20] Catalytic H_2 production at negative potentials may cause deviations from the equilibrium scheme suggested in Figure 3. As addressed in the SI, this deviation will in particular affect the extracted potential associated with the H_{sred} state (E_4).

The fits to the equilibrium scheme are presented in Figure 2B–F with solid curves. It turns out that the midpoint potential for the H_{ox}/H_{red} transition is quite close to that of the $H_{red}H^+/H_{sred}H^+$ transition (i.e., E_1 = −375 ± 10 mV and E_4 = −418 ± 20 mV). This is not surprising because both transitions involve the same reduction event of the $[4Fe–4S]_H$ subcluster. Due to the deviation from equilibrium at low potentials (see SI), the fitted $|E_4|$ value will be overestimated and the difference between E_1 and E_4 becomes even smaller.

The pH dependence of the H_{ox}/H_{red} and H_{red}/H_{sred} transitions is mainly determined by the $H_{red}/H_{red}H^+$ protonation event modeled with a pK_{red} = 7.2 ± 0.2. Due to the limited available pH range (6.0–10.0), the pK_{ox} parameter could adopt a range of values (pK_{ox} = 1.0–5.0).

The spectro-electrochemical experiments in Figure 2B–F can also be fitted individually for every pH to the three-state model previously used to extract the midpoint potentials $E(H_{ox}/H_{red})$ and $E(H_{red}/H_{sred})$, where H_{red} represents the sum of both reduced states[9,13,14] The individual fits are presented in figure S6 (SI) and the extracted potentials are summarized in Figure 4 (inset and data points). The pH dependence of the three-state midpoint potentials $E(H_{ox}/H_{red})$ and $E(H_{red}/H_{sred})$ can be calculated from the six-state parameters (pK_{ox}, pK_{red}, pK_{sred}, E_1…E_4) combined with the pH value.[20]

$$E(H_{ox}/H_{red}) = E_1 - \frac{RT}{F}\ln\left\{\frac{1 + 10^{(pKox-pH)}}{1 + 10^{(pKred-pH)}}\right\} \quad (3)$$

$$E(H_{red}/H_{sred}) = E_2 - \frac{RT}{F}\ln\left\{\frac{1 + 10^{(pKred-pH)}}{1 + 10^{(pKsred-pH)}}\right\} \quad (4)$$

Figure 4 shows that for extreme pH values the midpoint potentials reach plateau values at the "intrinsic" midpoint potentials E_1, E_2, E_3, and E_4. Because the value for E_3 is dependent on pK_{ox}, which is poorly defined, this plateau value is also inaccurate as demonstrated by the multiple curves calculated for different pK_{ox} all fitting the data satisfactorily (inset and data points). Figure 4 shows that the difference between $E(H_{ox}/H_{red})$ and $E(H_{red}/H_{sred})$ is smallest when the pH is close to the pK_{red} value (7.2). This may explain why for

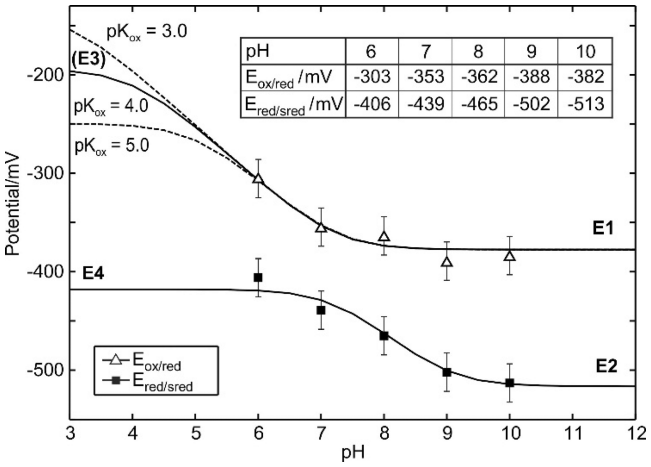

pH	6	7	8	9	10
$E_{ox/red}$ /mV	-303	-353	-362	-388	-382
$E_{red/sred}$ /mV	-406	-439	-465	-502	-513

Figure 4. Experimental pH dependence of the three-state $E_{ox/red}$ and $E_{red/sred}$ midpoint potentials as determined by the fits in Figure S6 (symbols and inset table) as compared to the pH dependence based on the six-state model (Figure 3) and eqs 1–4. For pK_{ox}, only the upper limit (<5.0) can be given. Fit parameters: pK_{red} = 7.2 ± 0.2, pK_{sred} = 9.0 ± 0.2, E_1 = −377 ± 10 mV, E_4 = −417 ± 10 mV. E_2 = −520 mV (using eq 2). Using eq 1, we arrive at the plateau values for E_3 depending on the value of pK_{ox}.

*Cr*HydA1 the two midpoint potentials (at pH 8.0) are closer together (−362 and −465 mV) than for the [FeFe] hydrogenase of *D. desulfuricans* (−395 vs −540 mV).[14] Because at pH 8.0 the H-cluster of *Dd*HydAB almost exclusively shows the $H_{red}H^+$ species, its pK_{red} parameter must be substantially larger than 8.0.

The current FTIR spectro-electrochemical study on *Cr*HydA1 suggest that the first steps in the catalytic (proton reduction) cycle are characterized by a sequential "ECE" mechanism linking $H_{ox} + e^- \rightarrow H_{red} + H^+ \rightarrow H_{red}H^+ + e^- \rightarrow H_{sred}H^+$. However, kinetics under turnover may follow a different EC order at extreme pH values or potentials. The ECE mechanism is appealing because both redox events occur at a potential close to the equilibrium H^+/H_2 potential at pH 7 (≈ −400 mV assuming 1 bar H_2), and the proton transfer between the two H_{red} states has a pK_a of ≈7. This would provide a smooth energy landscape throughout the catalytic cycle, which is required for efficient reversible catalysis. The hydrogen exposure experiment described in the SI (Figure S5) confirmed that the enzyme is in equilibrium with both the H^+/H_2 couple and the electrode/mediators system at the corresponding potentials. As can be seen in Figure 2B–F, the potential at which the catalytically competent H_{sred} state starts to be populated is always close to the hydrogen potential with the best match at pH 7. This correlates nicely with the pH dependent activity of the enzyme (Figure S1).

Protonation of H_{red} triggers electronic rearrangement to form $H_{red}H^+$, probably through a charge neutralization effect. Such an event involving the $[4Fe–4S]_H$ subcluster has been previously described in a DFT study on the possible hydride states in the catalytic mechanism[21] as well as in a study on inorganic mimics of the H-cluster.[15] The current study provides the first experimental support of this mechanism. The updated working model of the catalytic cycle[4] is presented in Scheme 1.

We speculate that a similar internal PCET step is involved in the stabilization of the putative terminal hydride in the catalytic cycle upon binding of H_2 to H_{ox}. In such a scenario, H_2 is heterolytically split, the proton is captured in the ADT bridge

DOI: 10.1021/jacs.6b12636
J. Am. Chem. Soc. 2017, 139, 1440–1443

Scheme 1. Proposed Catalytic Cycle Including Proton Coupled Electronic Rearrangement between H_{red} and $H_{red}H^{+}$[a]

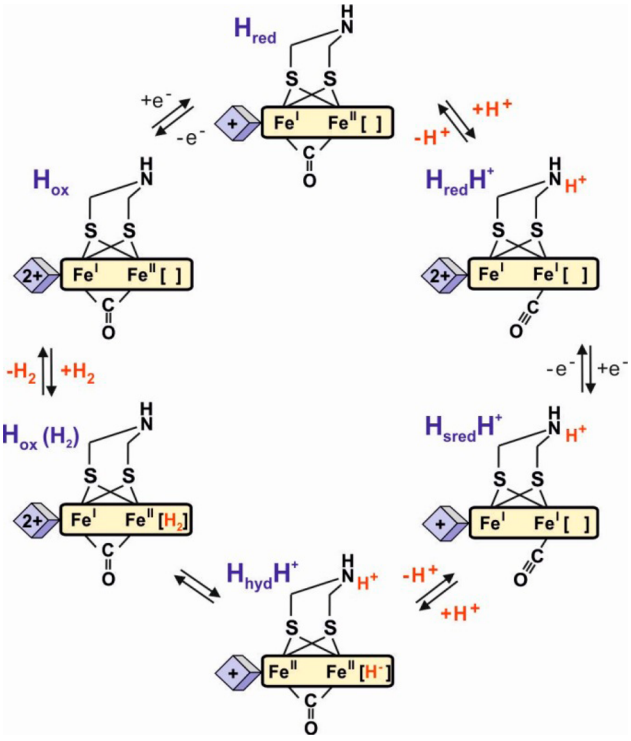

[a]A similar internal step is assumed upon H_2 formation/splitting between $H_{hyd}H^{+}$ and $H_{ox}(H_2)$.

while the hydride is stabilized on the distal iron of the $[2Fe]_H$ subsite in concert with electron transfer from $[2Fe]_H$ to $[4Fe–4S]_H$ (see Scheme 1 and Figure S7). Taking into account the highly conserved structure of the H-cluster in both bacterial and eukaryotic [FeFe] hydrogenases,[22] it is likely that the proton coupled electronic rearrangement described here is valid for all [FeFe] hydrogenases.

■ ASSOCIATED CONTENT

Supporting Information

The Supporting Information is available free of charge via the Internet at The Supporting Information is available free of charge on the ACS Publications website at DOI: 10.1021/jacs.6b12636.

Material and Methods; pH dependent enzyme activity; mediators used; FTIR bands overview; electrochemical titrations under equilibrium conditions; H_2 exposure experiment in ATR cell; treatment of a multiple-state chain of equilibria; three-state model; PCET as initial/final step in H_2 oxidation/production (PDF)

■ AUTHOR INFORMATION

Corresponding Authors

*Edward.Reijerse@cec.mpg.de
*Wolfgang.Lubitz@cec.mpg.de

ORCID

Wolfgang Lubitz: 0000-0001-7059-5327

Notes

The authors declare no competing financial interest.

■ ACKNOWLEDGMENTS

The authors thank Mr. Alaa Alsheikh Oughli for the synthesis of the −523 mV mediator (see SI). The Max Planck Society is gratefully acknowledged for financial support.

■ REFERENCES

(1) Lubitz, W.; Ogata, H.; Ruediger, O.; Reijerse, E. *Chem. Rev.* **2014**, *114*, 4081.
(2) Glick, B. R.; Martin, W. G.; Martin, S. M. *Can. J. Microbiol.* **1980**, *26*, 1214.
(3) Hatchikian, E. C.; Magro, V.; Forget, N.; Nicolet, Y.; Fontecilla-Camps, J. C. *J. Bacteriol.* **1999**, *181*, 2947.
(4) Adamska, A.; Silakov, A.; Lambertz, C.; Ruediger, O.; Happe, T.; Reijerse, E.; Lubitz, W. *Angew. Chem., Int. Ed.* **2012**, *51*, 11458.
(5) Adams, M. W. W. *Biochim. Biophys. Acta, Bioenerg.* **1990**, *1020*, 115.
(6) Pereira, A. S.; Tavares, P.; Moura, I.; Moura, J. J. G.; Huynh, B. H. *J. Am. Chem. Soc.* **2001**, *123*, 2771.
(7) Nicolet, Y.; de Lacey, A. L.; Vernede, X.; Fernandez, V. M.; Hatchikian, E. C.; Fontecilla-Camps, J. C. *J. Am. Chem. Soc.* **2001**, *123*, 1596.
(8) Nicolet, Y.; Lemon, B. J.; Fontecilla-Camps, J. C.; Peters, J. W. *Trends Biochem. Sci.* **2000**, *25*, 138.
(9) Adamska-Venkatesh, A.; Krawietz, D.; Siebel, J.; Weber, K.; Happe, T.; Reijerse, E.; Lubitz, W. *J. Am. Chem. Soc.* **2014**, *136*, 11339.
(10) Mulder, D. W.; Ratzloff, M. W.; Bruschi, M.; Greco, C.; Koonce, E.; Peters, J. W.; King, P. W. *J. Am. Chem. Soc.* **2014**, *136*, 15394.
(11) Greco, C.; Bruschi, M.; Fantucci, P.; Ryde, U.; De Gioia, L. *ChemPhysChem* **2011**, *12*, 3376.
(12) Esselborn, J.; Lambertz, C.; Adamska-Venkatesh, A.; Simmons, T.; Berggren, G.; Noth, J.; Siebel, J.; Hemschemeier, A.; Artero, V.; Reijerse, E.; Fontecave, M.; Lubitz, W.; Happe, T. *Nat. Chem. Biol.* **2013**, *9*, 607.
(13) Silakov, A.; Kamp, C.; Reijerse, E.; Happe, T.; Lubitz, W. *Biochemistry* **2009**, *48*, 7780.
(14) Roseboom, W.; De Lacey, A. L.; Fernandez, V. M.; Hatchikian, E. C.; Albracht, S. P. J. *J. Biol. Inorg. Chem.* **2006**, *11*, 102.
(15) Olsen, M. T.; Rauchfuss, T. B.; Wilson, S. R. *J. Am. Chem. Soc.* **2010**, *132*, 17733.
(16) Huynh, M. T.; Wang, W. G.; Rauchfuss, T. B.; Hammes-Schiffer, S. *Inorg. Chem.* **2014**, *53*, 10301.
(17) Dempsey, J. L.; Winkler, J. R.; Gray, H. B. *Chem. Rev.* **2010**, *110*, 7024.
(18) Yu, L.; Greco, C.; Bruschi, M.; Ryde, U.; De Gioia, L.; Reiher, M. *Inorg. Chem.* **2011**, *50*, 3888.
(19) Katz, S.; Noth, J.; Horch, M.; Shafaat, H. S.; Happe, T.; Hildebrandt, P.; Zebger, I. *Chem. Sci.* **2016**, *7*, 6746.
(20) Zu, Y. B.; Couture, M. M. J.; Kolling, D. R. J.; Crofts, A. R.; Eltis, L. D.; Fee, J. A.; Hirst, J. *Biochemistry* **2003**, *42*, 12400.
(21) Bruschi, M.; Greco, C.; Kaukonen, M.; Fantucci, P.; Ryde, U.; De Gioia, L. *Angew. Chem., Int. Ed.* **2009**, *48*, 3503.
(22) Vignais, P. M.; Billoud, B. *Chem. Rev.* **2007**, *107*, 4206.

DOI: 10.1021/jacs.6b12636
J. Am. Chem. Soc. 2017, 139, 1440–1443